Open Archive Toulouse Archive Ouverte

OATAO is an open access repository that collects the work of Toulouse researchers and makes it freely available over the web where possible

This is an author's version published in: http://oatao.univ-toulouse.fr/22982

To cite this version:

Franc, Jacques and Debenest, Gérald and Jeannin, Laurent and Ababou, Rachid and Masson, Rolland Comparisons of FV-MHMM with other finite volume multiscale methods. (2018) Transport in Porous Media, 125 (2). 151-171. ISSN 0169-3913.

Any correspondence concerning this service should be sent to the repository administrator: tech-oatao@listes-diff.inp-toulouse.fr

Comparisons of FV-MHMM with Other Finite Volume Multiscale Methods

Jacques Franc[1] · Gerald Debenest[1] · Laurent Jeannin[2] · Rachid Ababou[1] · Roland Masson[3]

Abstract

Upscaling and multiscale methods in reservoir engineering remain a complicated task espe-cially when dealing with heterogeneities. In this study, we focus on flow field problem with a

Darcy's equation considered at the fine scale. The main difficulty is then to obtain an accurate description of the flow behavior by using multiscale methods available in petroleum engineering. We cross-compare three of the main finite volume formulations: multiscale finite volume method (MsFv), multiscale restriction smoothed (MsRSB) and a new finite volume method, FV-MHMM. Comparisons are done in terms of accuracy to reproduce the fine scale behavior.

Keywords Upscaling · Multiscale method · Finite volume · Heterogeneity

1 Introduction

Upscaling and multiscale algorithms both serve the same aim of defining models that are able to capture global trends of the flow properties on a larger scale than the reference scale,

✉ Gerald Debenest
  debenest@imft.fr

  Jacques Franc
  jacques.franc@imft.fr

  Laurent Jeannin
  laurent.jeannin@storengy.com

  Rachid Ababou
  ababou@imft.fr

  Roland Masson
  Roland.MASSON@unice.fr

[1] INPT, UPS, IMFT (Institut de Mécanique des Fluides de Toulouse), Université de Toulouse, Allée Camille Soula, 31400 Toulouse, France

[2] Storengy, Bois-Colombes, France

[3] Laboratoire de Mathématiques J.A. Dieudonné, UMR 7351 CNRS, University Nice Sophia Antipolis, Nice, France

referred to as the fine scale. However, *upscaling* and *multiscale methods* differ when it comes to the treatment of the fine scale. *Upscaling* techniques, once they have averaged the flow properties, produce an upscaled equivalent model and deal with it at the large-scale. On the other hand, *multiscale methods* are designed to keep the fine scale information as they consider that a good accuracy cannot be achieved without it. Then, they will couple scales thanks to upgridding and downgridding steps.

For the methods that are in use in this study, the Darcy-to-Field scale upscaling will be considered. The generalized Darcy's law is considered as the fine scale model. This will give us the reference solution. *Multiscale algorithms* have been extensively studied, starting from the works of Hou and Wu on multiscale finite elements (Hou and Wu 1997) for Darcy-like equations.

On the one hand, the finite elements methods have known important developments with multiscale finite element methods (MsFEM) (Arbogast et al. 2000), numerical subgrid methods (Arbogast 2002; Arbogast et al. 2007) and more recently generalized multiscale finite element methods (GMsFEM) (Efendiev et al. 2013). These rely on the construction of local basis function that fits the underlying heterogeneities. Numerical subgrid methods are rather solving for averaged pressure values on the coarse scale and for its variation on subgrid scale.

On the other hand, the multiscale finite volume methods [MsFv (Jenny et al. 2003)] have been derived and designed to be locally and globally conservative. This work has been extended by introducing iterative algorithm to smooth multiscale approximate solutions (Hajibeygi et al. 2008). Later works have introduced other features to model density driven flows or flows with capillary forces by using correction functions (Lunati and Lee 2009; Lunati and Jenny 2006a; Hajibeygi and Jenny 2008; Jenny and Lunati 2009). More recently, an algebraic formulation of the method has been developed (Wang et al. 2014; Lee et al. 2009; Zhou et al. 2012). Its use as a preconditioner for Krylov-type iterative solvers has been investigated (Castelletto et al. 2017; Lunati et al. 2011; Manea et al. 2016). On another branch, the multiscale restriction smoothed basis [MsRSB (Møyner and Lie 2016)] has been developed. It takes its inspiration from extensive studies of MsFv algorithm and algebraic multigrid solvers (Vaněk et al. 1996) introducing multiple time Jacobi smoothing on overlapping supports to construct its basis functions. An alternative method, finite volume multiscale hybrid mixed method [FV-MHMM (Franc et al. 2017)] has been proposed. It is based on the family of multiscale hybrid mixed finite element methods introduced in Harder et al. (2013) which has been adapted to finite volume formulation.

This paper intends to cross-compare the above-mentioned finite volume multiscale methods, i.e., the multiscale finite volume method (MsFv), the multiscale restriction smoothed basis method (MsRSB) and the finite volume multiscale hybrid mixed method (FV-MHMM). The first section will give more details about the considered three methods. In a second section, the performance of each method on 2D layers of the 10th SPE (Christie et al. 2001) test case will be compared. As a last test case, a slanted permeability field will be considered.

2 Methods Description

In this section, we describe briefly the three finite volume methods used to study multiscale problems for fluid flow in heterogeneous media. For single-phase incompressible flows, pressure field equation over the domain Ω follows the Darcy's equation:

$$\nabla \cdot (K(\mathbf{x})\nabla p) = -\mathrm{f} \text{ in } \Omega, \tag{1}$$

where $K(\mathbf{x})$ stands for the permeability field which is heterogeneously distributed over Ω, and f a general source term. Boundary conditions are needed and are defined according to the following equations.

$$(K(\mathbf{x})\nabla p) \cdot \mathbf{n}_{\partial\Omega} = g \text{ on } \partial\Omega_{\mathrm{N}},$$
$$p = p^g \text{ on } \partial\Omega_{\mathrm{D}},$$

where $\mathbf{n}_{\partial\Omega}$ stands for the unit normal vector to the boundary $\partial\Omega$ outward to Ω, and $\overline{\partial\Omega_{\mathrm{D}}} \cup \overline{\partial\Omega_{\mathrm{N}}} = \partial\Omega$, $\partial\Omega_{\mathrm{D}} \cap \partial\Omega_N = \emptyset$. The first equation is a classical Neumann boundary condition with prescribed flux g on $\partial\Omega_{\mathrm{N}}$, whereas the second one is a Dirichlet boundary condition with imposed pressure p^g on $\partial\Omega_{\mathrm{D}}$.

Herein, we focus on the finite volume methods available and we briefly recall the systems of equations to be solved in each of them.

2.1 FV-MHMM

Let M_H be the set of coarse cells K partitioning the domain Ω, F_H be the set of coarse faces, and ∂K denote the boundary of a coarse cell K with its unit normal vector $\mathbf{n}_K$ oriented outward to K.

Starting from the primal hybrid formulation of Raviart and Thomas (1977a, b), Harder et al. (2013, 2015) explain how to construct a multiscale method sharing the same idea that flux continuity between cells (here coarse scale cells) can be enforced weakly using Lagrange multipliers λ. It is formulated as:

find $(p, \lambda) \in V \times \Lambda$ such that:

$$\int_\Omega K(\mathbf{x})\nabla p \cdot \nabla q \mathrm{d}\mathbf{x} + \sum_{K \in M_H} \int_{\partial K} \lambda \mathbf{n} \cdot \mathbf{n}_K \, q|_K \mathrm{d}\sigma$$
$$+ \sum_{K \in M_H} \int_{\partial K} \mu \mathbf{n} \cdot \mathbf{n}_K \, p|_K \mathrm{d}\sigma \quad \text{for all } (q, \mu) \in V \times \Lambda,$$
$$= \int_\Omega f v \mathrm{d}\mathbf{x} + \int_{\partial\Omega} \mu \, p^g \mathrm{d}\sigma \tag{2}$$

where V is the broken Sobolev space $H^1(M_H)$ defined as:

$$H^1(M_H) = \{v \in L_2(\Omega) : \, v|_K \in H^1(K), \, K \in M_H\}, \tag{3}$$

Λ stands for the following Lagrange multipliers space

$$\Lambda := \left\{ \mu \in \prod_{K \in M_H} H^{-\frac{1}{2}}(\partial K) : \exists \boldsymbol{\sigma} \in H_{\mathrm{div}}(\Omega) \text{ s.t. } \mu|_{\partial K} = \boldsymbol{\sigma} \cdot \mathbf{n}|_{\partial K}, \, K \in M_H \right\}, \tag{4}$$

∇v is the broken gradient equal to $\nabla v|_K$ on each coarse cell $K \in M_H$, and $H^{-\frac{1}{2}}(\partial K)$ is the dual space of the space $H^{\frac{1}{2}}(\partial K)$ spanned by the traces on ∂K of functions in $H^1(K)$.

Let then split the space V orthogonally as:

$$V = V_0 \oplus \Pi_{K \in M_H} W_K,$$

where V_0 is the space of piecewise constant functions on each coarse cell $K \in M_H$ and W_K is the subset of null mean function over $H^1(K)$. This definition introduces the two-scale modeling scheme.

At fixed Lagrange multiplier λ, the fine scale solution in W_K defined by Eq. (2) decouples. It is obtained by superposition of the solutions of two local problems, a *local lambda problem* for Lagrange multipliers-driven effects and a *local source problem* for source-driven effects. They, respectively, read:

Find $\tilde{p}_K \in W_K$ such that:

$$\int_K K(\mathbf{x})\nabla\tilde{p}_K \cdot \nabla\tilde{q}_K \, d\mathbf{x} + \int_{\partial K} \lambda\mathbf{n} \cdot \mathbf{n}_K \tilde{q}_K \, d\sigma = 0 \quad \text{for all } \tilde{v}_K \in W_K, \tag{5}$$

Find $\tilde{p}_K \in W_K$ such that:

$$\int_K K(\mathbf{x})\nabla\tilde{p}_K \cdot \nabla\tilde{q}_K \, d\mathbf{x} = \int_K f\tilde{q}_K \, d\mathbf{x} \quad \text{for all } \tilde{v}_K \in W_K, \tag{6}$$

setting $\tilde{p}_K = T_K\lambda$ and $\tilde{p}_K = \hat{T}_K f$.

The coupling of the local fine scale solutions is obtained using Eq. (2) with test functions in $V_0 \times \Lambda$ to compute the Lagrange multiplier λ and the mean values in the coarse cells. It is formulated as follows using the previous solutions of the *local* problems $T_K\lambda$ and $\hat{T}_K f$ for all coarse cells $K \in M_H$:

Find $p_{0,K} \in \mathbb{R}$, $K \in M_H$ and $\lambda \in \Lambda$ such that:

$$\begin{cases} \sum_{K \in M_H} \int_{\partial K} \lambda\mathbf{n} \cdot \mathbf{n}_K \, d\sigma = \int_K f \, d\mathbf{x} \quad \text{for all } K \in M_H, \\ \sum_{K \in M_H} \int_{\partial K} \mu\mathbf{n} \cdot \mathbf{n}_K \left(p_{0,K} + T_K\lambda + \hat{T}_K f \right) d\sigma = \int_{\partial\Omega} \mu u_g \quad \text{for all } \mu \in \Lambda. \end{cases} \tag{7}$$

This multiscale algorithm is here implemented using a TPFA scheme for the local problems on each coarse cell K and by replacing the space Λ by a subspace Λ_H. In the following test cases, the vector space Λ_H will be typically defined as the vector space of polynomials $\mathbb{P}_l(\sigma)$ of degree l on each coarse face $\sigma \in F_H$. These choices of Λ_H will be denoted by Λ_l, $l = 0, 1, 2$ in the following sections. These polynomial spaces can also be weighted using harmonic averaging of the permeability field on each fine face of F_H as described in the following section. Readers can refer to Franc et al. (2017) for further details.

As an illustration, a typical basis function is reported, respectively, in Fig. 3a.

Once these basis functions are computed and the global system Eq. (7) solved, the approximate fine scale pressure $p^{\text{fv-mhmm}}(x)$ is interpolated as a linear combination of the coarse cell pressures as follows:

$$p(\mathbf{x}) \approx p^{\text{fv-mhmm}}(\mathbf{x}) = \sum_{K \in M_H} \left[p_{0,K} + \sum_{\sigma \in F_{H,K}} \left(T_K\lambda + \hat{T}_K f \right) \right] \tag{8}$$

Now, we will briefly recall the MsFv method.

2.2 MsFv

The multiscale method multiscale finite volume (MsFv) (Jenny et al. 2003) is constructed using two different meshes. A primal coarse grid is defined by partitioning a fine grid as usual in multiscale methods (solid line on Fig. 1). Then, a dual coarse grid is constructed, joining the cell centers of the primal grid (dashed lines in Fig. 1). The basis functions will be evaluated on this staggered dual grid. Those basis functions are useful to calculate equivalent

Fig. 1 MsFv: primal grid (full lines) dual grid (dashed lines)
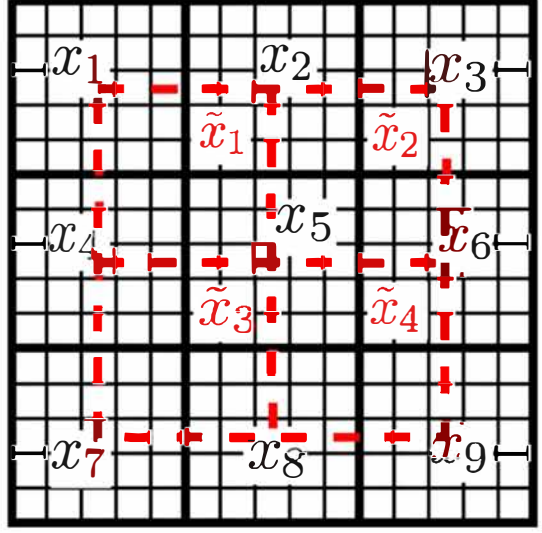
transmissivities (see Fig. 3b). Those meshes are superimposed to a fine mesh grid, capturing the details of the fine scale properties.

We now briefly recall the first three steps of the construction regarding the calculation of the coarse pressure. A remaining step deals with conservative fine scale velocity field reconstruction which is required to couple the flow with a transport equation.

Let us consider a *primal coarse grid* denoted by M_H with coarse cells $K \in M_H$ of cell center x_K. At each vertex $x_{\tilde{K}}$ of the primal grid, a dual coarse cell denoted by $\tilde{K}$ is built joining the neighboring cell centers x_K, $K \in M_{\tilde{K}}$, where $M_{\tilde{K}}$ denote the set of primal coarse cells sharing the vertex $x_{\tilde{K}}$. This defines the *dual coarse grid* $\tilde{M}_H$ as the set of dual coarse cells $\tilde{K} \in \tilde{M}_H$. Let us also denote by $x_{\tilde{K}}$, $\tilde{K} \in \tilde{M}_K$ the vertices of the cell K.

The first step is to build the basis functions $\bar{\Phi}_K^{\tilde{K}}$, $K \in M_{\tilde{K}}$ (Fig. 3b) on each dual coarse cell $\tilde{K}$. The second step is the computation of the correction functions $\bar{\Phi}_*^{\tilde{K}}$ for all $\tilde{K} \in \tilde{M}_H$. Both sets of basis functions are used to interpolate the pressure as a linear combination of the primal coarse cell pressures $\bar{p}_K$, $K \in M_H$. This allows to express the fluxes on the primal coarse cell faces as linear combinations of the primal coarse cell pressures. Then, in the third step, the linear system for the primal coarse cell pressures is obtained from the conservation equations written on the primal coarse cells.

For each $\tilde{K} \in \tilde{M}_H$, the basis functions $\Phi_K^{\tilde{K}}$, $K \in M_{\tilde{K}}$ are solutions of the following equations set on the dual coarse cell $\tilde{K}$ with value $\delta_{K,L}$ at the vertices x_L, $L \in M_{\tilde{K}}$ of the dual coarse cell $\tilde{K}$:

$$\begin{cases} \nabla \cdot \mathbf{K}(x) \nabla \Phi_K^{\tilde{K}} = 0 & \text{in } \tilde{K}, \\ \nabla_{\perp} \cdot \mathbf{K}(x) \nabla \Phi_K^{\tilde{K}} = 0 & \text{on } \partial \tilde{K}, \\ \Phi_K^{\tilde{K}}(x_L) = \delta_{K,L}, & L \in M_{\tilde{K}}. \end{cases} \tag{9}$$

The addition of a second kind of basis functions, *correction basis functions*, is set to model inhomogeneous part of the multiscale approximation of the fine scale pressure, introducing $\Phi_*^{\tilde{K}}$ whose definition reads:

$$\begin{cases} \nabla \cdot \mathbf{K}(\mathbf{x}) \nabla \Phi_*^{\widetilde{K}} = f & \text{in } \widetilde{K}, \\ \nabla_{\perp} \cdot \mathbf{K}(\mathbf{x}) \nabla \Phi_*^{\widetilde{K}} = 0 & \text{on } \partial \widetilde{K}, \\ \Phi_*^{\widetilde{K}}(\mathbf{x}_L) = 0, & L \in M_{\widetilde{K}}. \end{cases} \quad (10)$$

It has to be noted that the correction functions are no more in use among the MsFv community nowadays (Ţene et al. 2015), but are presented as originally part of the method. Once these basis functions are computed, the approximate fine scale pressure $p^{\mathrm{msfv}}(x)$ is interpolated as a linear combination of the primal coarse cell pressures as follows:

$$p(\mathbf{x}) \approx p^{\mathrm{msfv}}(\mathbf{x}) = \sum_{K \in M_H} \bar{p}_K \left[\sum_{\widetilde{K} \in \widetilde{M}_K} \Phi_K^{\widetilde{K}}(\mathbf{x}) \right] + \sum_{\widetilde{K} \in \widetilde{M}_H} \Phi_*^{\widetilde{K}}(\mathbf{x}) \quad (11)$$

and the primal coarse cell pressures $\bar{p}_K$, $K \in M_H$ are obtained from the conservation equations in each primal coarse cell K defining the set of linear coarse scale equations.

If one would like to add, sink terms, gravity or capillary effects, new basis functions have to be defined, denoted as correction functions in the system of basis functions calculations [see Lunati and Jenny (2008) or Jenny and Lunati (2009)]. An iterative scheme can also be applied in order to reduce the error which happened at *dual* coarse cells' boundaries. For multiphase flow, a conservative fine scale velocity field is required and an extra step is then needed to ensure that p^{msfv} fulfills this requirement (Lunati and Jenny 2006b).

As a last method, we choose to report one of the most recent multiscale method MsRSB.

2.3 MsRSB

MsRSB method is inspired from the work on AMG solver (Vaněk et al. 1996). It takes advantages of overlapping areas between coarse cells to compute the needed basis functions (see Fig. 2). However, a particular treatment has to be done during smoothing iterative process for the fine cells included in these overlapping regions. This will enforce the partition of unity, and it will allow to build a conservative operator (see Fig. 3c). Let us define three different areas for defining the basis functions computation associated with a given coarse cell $K \in M_H$: I_K the overlap support, the overlap's boundary B_K and the global boundary inside the overlap region $G \cap I_K$ introducing G as the superposition of all the overlaps' boundaries, $G = \bigcup_K B_K$ (see Fig. 2).

Let F denote the set of fine cells. For convenience, we identify in the following the domains K, I_K, B_K and G with their corresponding subsets of fine cells. Starting from the prolongation operator defined for all fine cells $i \in F$ as $P_{i,K}^1 = 1$, $i \in K$ and $P_{i,K}^1 = 0$, $i \notin K$ and smoothing it using n relaxed Jacobi iterations, the algorithm then reads for $\nu = 1, n$:

Starting from the prolongation operator defined for all fine cells $i \in F$ as $P_{i,K}^1 = 1$, $i \in K$ and $P_{i,K}^1 = 0$, $i \notin K$ and smoothing it using n relaxed Jacobi iterations, the algorithm then reads for $\nu = 1, n$:

1. Compute the relaxed Jacobi update with $\omega = 2/3$ optimal value for Poisson-like equation for I_K, for each area K

$$\hat{d}_{i,K} = -\omega \sum_{j \in F} (D^{-1}(A - D))_{i,j} P_{j,K}^{\nu} \quad (12)$$

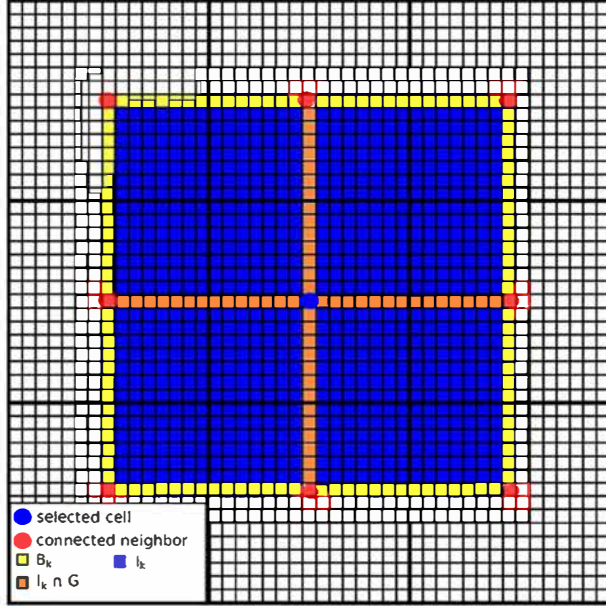with A the fine grid operator and D its diagonal.

Fig. 2 MsRSB: definition of mesh elements, different areas, and boundaries used
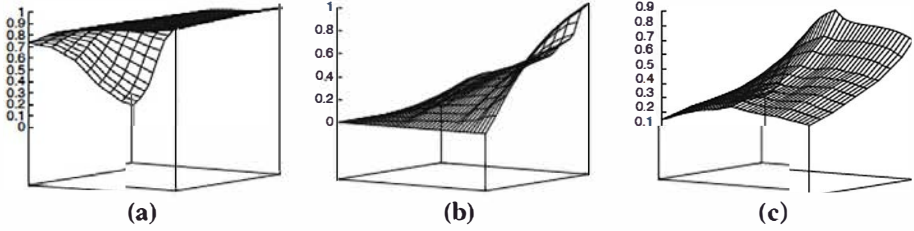

      (a)   (b)   (c)

Fig. 3 Illustration of basis function for **a** FV-MHMM, **b** MsFv and **c** MsRSB

2. Correct on the overlapping areas, introducing $H_i = \{K \mid i \in I_K\}$ collection of coarse owner's indexes of a fine cell $i \in G$

$$
d_{i,K} =
\begin{cases}
\hat{d}_{i,K}, & i \in I_K \backslash G, \\[2mm]
\dfrac{\hat{d}_{i,K} - P^{\nu}_{i,K} \sum\limits_{k \in H_i} \hat{d}_{ik}}{1 + \sum\limits_{k \in H_i} \hat{d}_{ik}}, & i \in I_K \cap G, \\[2mm]
0, & i \notin I_K
\end{cases}
\tag{13}
$$

3. Update $P^{\nu+1}_{i,K} = P^{\nu}_{i,K} + d_{i,K}$, $i \in F$, and evaluate the error $e_K = \max\limits_{i \in I_K \backslash G} (|\hat{d}_{i,K}|)$ on the internal support. Terminate if $e_K < tol$ and set $P_{i,K} = P^{\nu+1}_{i,K}$, $i \in F$.

The fine scale approximate pressure is then obtained as the following linear combination of the coarse cell pressures $\bar{p}_K$, $K \in M_H$

$$
p^{\text{MsRSB}}(x) = \sum_{K \in M_H} \bar{p}_K P_{i,K} \text{ for all } x \in i, \ i \in F.
$$

and the coarse scale system is obtained from the conservation equations in each coarse cell $K \in M_H$.

3 Methods Improvement

Dealing with highly heterogeneous permeability fields exhibiting higly connected path is problematic for such methods. Both MsFv and MsRSB methods have known significant improvements since they were derived (Hajibeygi et al. 2008, 2010; Hajibeygi and Jenny 2011; Lunati and Jenny 2008; Wang et al. 2014). One of the most notable is to use several cycles successively smoothing and solving via multiscale methods to converge to the fine scale results.

The FV-MHMM does not implement such a technique. But two types of weighting schemes are proposed in this section in order to enhance its solution accuracy.

Let p_{ms} denote the approximation of the fine scale pressure and p_{c} be the coarse scale solution obtained by the multiscale method (without mention of the multiscale method). Let us introduce the operator notation of Eq. (1) as

$$Ap = b \tag{14}$$
$$A_{\mathrm{c}} p_{\mathrm{c}} = Rb. \tag{15}$$

With P the prolongation operator based on the basis function computed in MsFv or MsRSB and R the restriction operator as described in Møyner and Lie (2016). The coarse scale operator A_{c} is then related to the fine scale operator A, in such a way as:

$$R(Ap_{\mathrm{ms}}) = RA(Pp_{\mathrm{c}}) = A_{\mathrm{c}} p_{\mathrm{c}}. \tag{16}$$

Using this multigrid formulation, an iterative form of these two methods can be written.

3.1 MsFv and MsRSB iterative formulation

Both MsFv and MsRSB can be used in smoother-multiscale cycle as mentioned in Algorithm 1.

Let us denote the *multiscale residuals* $R_{\mathrm{ms}}^{\nu-1} = b - Ap_{\mathrm{ms}}^{\nu-1}$, which measures the discrepancy from the reconstructed multiscale solution p_{ms} to the finite volume solution $A^{-1}b$.

with $f_{\mathrm{smooth}}(z)$ implementing either a Jacobi smoother or an ILU_0 factorization with 0 level of fill-in. The use of different smoothing functions leads both MsFv and MsRSB to different convergence behavior. The optimal number of smoothing iterations n_{smooth} has been reported to be approximatively the number of coarsening ratio (Ţene et al. 2015, 2016). The cases reported in Fig. 4 are simulations over the two type of facies found in the layers in 10th SPE case. They are performed setting a tolerance stopping criteria on the residuals to 10^{-12} and a 10×11 coarses cells onto the 60×220 fine cells discretization.

In Fig. 4a, for the log-normally distributed facies, the convergence of the Jacobi and ILU_0 smoothers is comparable but allows lower error reduction with respect to the number of iterations.

In Fig. 4b, it can be seen, as reported in Møyner and Lie (2016), Wang et al. (2014), that the MsFv methods can struggle to find a solution on such channelized medium. It can be corrected choosing larger blocks to fit more heterogeneous features into the coarse blocks. Switching to a 5×11 coarse discretization allows to find a converged MsFv solution but implies a lower accuracy for the MsRSB solution. This configuration is reported in Fig. 4c.

Algorithm 1 Smoother-multiscale solution cycle description

Let be $f_{c2f}(z) = P(A_c^{-1} Rz)$ and $f_{smooth}(z)$.

1. Construct a first multiscale approximation of the fine scale pressure using:

$$p_{ms}^0 = f_{c2f}(b)$$

2. if [iterations are demanded <u>and</u> a smoother is provided], for ν iterations times (or before if residual is small enough w.r.t tolerance)

   (a) apply n_{smooth} iteration of smoothing of the multiscale residual

   $$p_{ms}^{\nu-1} = f_{smooth}\left(R_{ms}^{\nu-1}\right)$$

   (b) update p_{ms}^ν by solving such as,

   $$p_{ms}^\nu = p_{ms}^{\nu-1} + f_{c2f}\left(R_{ms}^{\nu-1}\right)$$

(a)

(b)   (c)
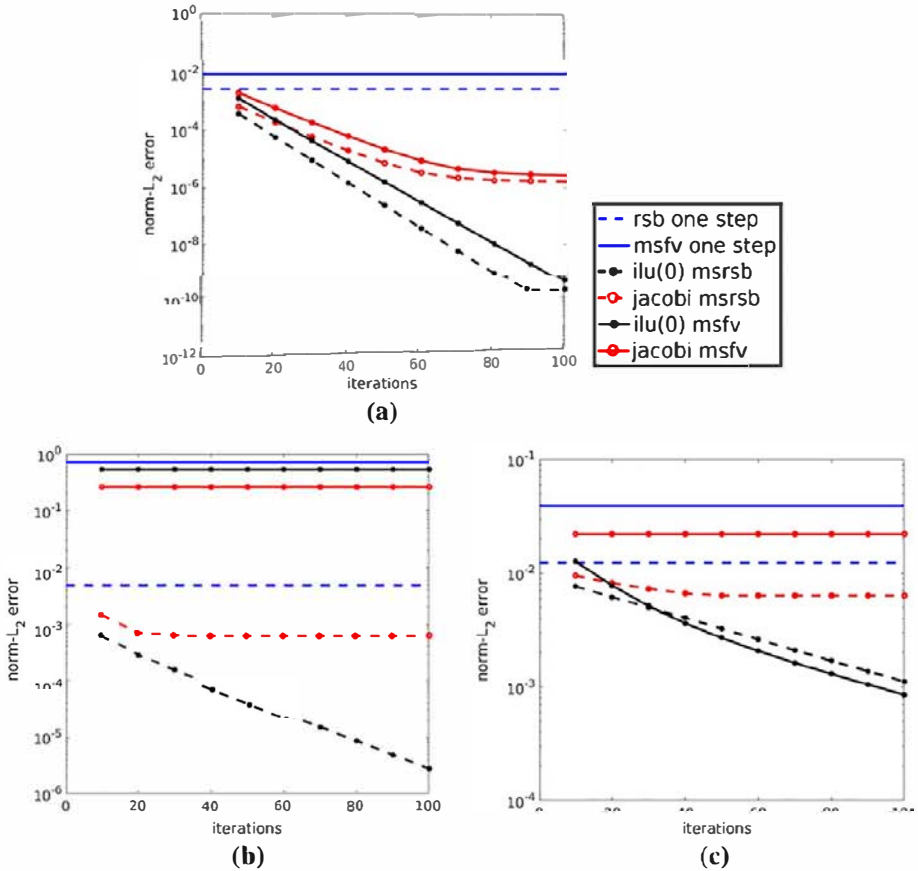
Fig. 4 Convergence behavior considering Jacobi or ILU_0 smoother. Dotted lines stand for MsRSB method; solid lines are for MsFv method. Behavior a for the 13th SPE10 test case with a 10×11 coarse mesh, b for the 84th SPE10 test case with a 10×11 coarse mesh and c for a 5×11 coarse mesh. Blue lines represent for each multiscale methods, the error level, as if they are considered as a single stage multiscale solver (corresponding to step 1 in Algorithm 1)

Jacobi is then limited as the fine scale operator has important off-diagonal coefficients. As in Møyner and Lie (2016), Wang et al. (2014), the ILU_0 smoother will be chosen when operating smoother-multiscale solution cycles with these methods.

3.2 FV-MHMM Weighting Schemes

The definition of a weighting schemes is crucial for the FV-MHMM as previously described in Franc et al. (2017). This is particularly important where the permeability field has both high contrast in the values in a short distance range and long correlated features whose characteristic lengths are larger than the size of a coarse cell. Two of them are described in the following subsections.

3.2.1 Transmissivity Weighting (tw) Scheme

For the FV-MHMM, according to Franc et al. (2017), we can weight the functions of $\mathbb{P}_l(\sigma)$ to produce a new space that is piecewise adapted to the neighbor transmissivities of the selected coarse face. Let us define the transmissivity weighting scheme (tw) for $\sigma \in F_H$:

- $F_{h,\sigma}$ denotes the set of fine faces of σ
- T_e denote the transmissivity of the fine face $e \in F_{h,\sigma}$.

Let the function λ_σ be defined on σ such that

$$\lambda_\sigma(\mathbf{x}) = \frac{T_e}{\sum_{e \in F_{h,\sigma}} T_e} \text{ for all } \mathbf{x} \in e, \ e \in F_{h,\sigma}.$$

Then, the weighted space Λ_l is spanned on each coarse faceσ by $\lambda_\sigma \mathbb{P}_l(\sigma)$.

3.2.2 MultiScale Two Point Flux Approximation (mstpfa) Scheme

Another adaptation can be inspired from Møyner and Lie (2014), Aarnes (2004). Performing a local simulation of an imposed flux through the coarse face, the heterogeneous fine scale fluxes along the coarse face can be used to build a weighting scheme. Let us define a multiscale two point flux approximation weighting scheme (mstpfa) for $\sigma \in \overline{F_H}$, $\overline{F_H} \cap \partial\Omega = \varnothing$:

- $F_{h,\sigma}$ denotes the set of fine faces of σ
- ϕ_e denote the flux of the fine face $e \in F_{h,\sigma}$.

Let the function λ_σ be defined on σ such that

$$\lambda_\sigma(\mathbf{x}) = \frac{\phi_e}{\sum_{e \in F_{h,\sigma}} \phi_e} \text{ for all } \mathbf{x} \in e, \ e \in F_{h,\sigma}.$$

Then, the weighted space Λ_l is spanned on each coarse faceσ by $\lambda_\sigma \mathbb{P}_l(\sigma)$.

In the next section, a focus will be done on the accuracy of each method compared to different facies. As an indicator, we will compare the fine scale solution to the multiscale ones. The accuracy with respect to the fine grid finite volume solution will be assessed using the following error measures:

$$\epsilon_{L_2} = \frac{||p_{\text{ms}} - p_{ref}||_2}{||p_{\text{ref}}||_2} \tag{17}$$

$$\epsilon_1(\mathbf{x}) = \frac{|p_{\text{ms}}(\mathbf{x}) - p_{\text{ref}}(\mathbf{x})|}{p_{\text{ref}}^{\max} - p_{\text{ref}}^{\min}}, \ \mathbf{x} \in \Omega. \tag{18}$$

The first indicates the overall level of error, while the second plotted in colormap mode will allow us to correlate the errors with the mesh and/or the permeability field features. Whether use of weighted version or native of FV-MHMM, quadratic polynomial space will be used to approximate Λ_H (i.e., use of Λ_2). An ILU_0 smoother will be used when dealing with smoother-multiscale methods cycle implementation, denoted as improved version for MsFv and MsRSB. In the next section, MRST2016 Toolbox (Lie 2014) will be used when considering tests for both MsFv and MsRSB methods.

4 The 10th SPE Case

The first test involves 2D layers of the 3D heterogeneous permeability field that has been generated for the 10th SPE benchmark [see Christie et al. (2001)]. It is a well-known test case that produces two main facies characteristics. On the 35 first layers, Tarbert formation types have been generated. Those layers are characterized by correlated log-normally distributed permeability values with high contrasts but moderate correlation lengths with respect to the size of the domain. On the remaining 50 layers, a fluvial Upper-Ness type has been generated. Those are channelized, i.e., the correlation length is of the size of the global domain extent. It produces very challenging permeability fields to perform upscaling on, as the scale separation assumption is not fulfilled. In a first step, native version of each multiscale method will be tested on different layers. In a second step, some improvement techniques will be taken into account and the error levels reported.

The two layers we select to perform this study are the 13th layer, for the top layers, and 84th layer, for the bottom layers. Once again they are chosen because they correspond, respectively, to two different permeability backgrounds, with different correlation lengths. Their log-permeability maps are reported in Fig. 5.

Dealing with the channelized typed layers, MsFv struggles to converge as explained in Møyner and Lie (2016), Wang et al. (2014). Nonetheless, a converged result can be obtained coarsening the coarse mesh, including more heterogeneous features in the same coarse cell. It is then decided to run tests with a 5×11 and 10×11 coarse meshes. Such a coarsening will result in a loss of accuracy for both MsFv and FV-MHMM. The coarse discretization 5×11 is chosen when reporting $\epsilon_1(\mathbf{x})$ as colormap.

For the numerical test cases, we define the following conditions reported in Table 1.

4.1 Native Versions of Multiscale Solvers

In this section, all the methods are used as direct solver. That is to say, with considering only the first stage of Algorithm 1 for MsFv and MsRSB. For FV-MHMM, it excludes any weighting schemes.

From Fig. 6a, the reader can notice that all methods localized their error peaks in the impermeable area at the top of the layer. From the L_2-norm error reported in Table 2a, it can be observed that the FV-MHMM in this configuration produces one order of magnitude lower error.

Switching to the channelized 84th layer, as the MsFv produces locally $\epsilon_1(\mathbf{x})$ error measures greater than 1, the scale is limited to the second largest value (which is obtained for FV-MHMM). From Fig. 6b, it can be observed that each methods produces their maximum errors, where impermeable features appear in the highly permeable channels. As confirmed
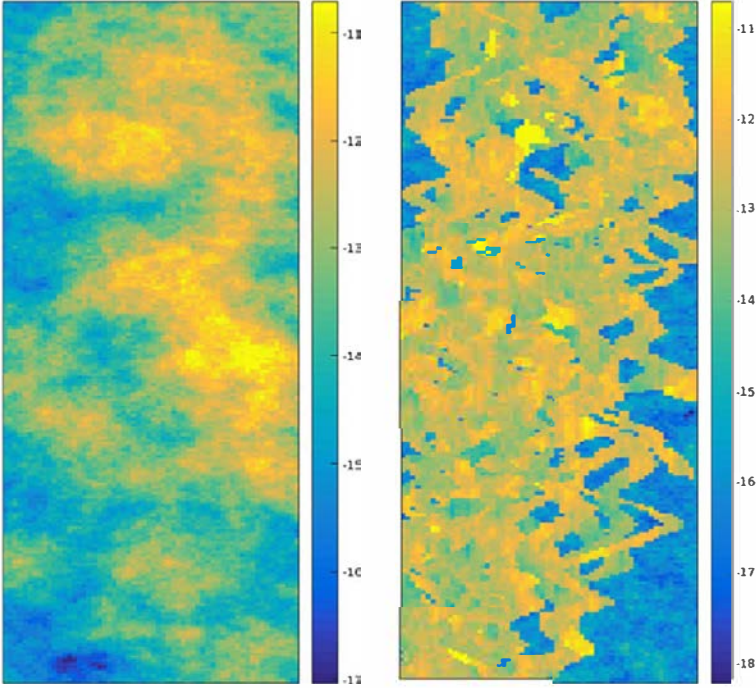
Fig. 5 Log-permeability field on the 13th and 84th layers

Table 1 Simulation conditions for SPE 10th test case		
Physics dim.		$1200\,\text{ft} \times 2200\,\text{ft}$
Fine grid		$60 \times 220\text{cells}$
Coarse grids		$(5, 10) \times 11\,\text{cells}$
Boundary cdt		$\Delta p = 1\,\text{Pa}$

by the L_2-norm error report in Table 2b, MsRSB produces the most accurate result on that facies with five times lower error level.

Repeating these tests on several layers along the 10th SPE test case, ϵ_{L_2} measures are represented in Fig. 7, while statistical report per facies is reported on Table 3. The same observation can be generalized. MsRSB is the most accurate method for channelized media, as it can benefit from the overlapping definitions in its basis functions construction. It includes more effects from the highly connected paths, whereas FV-MHMM, which has independently constructed basis functions, is then limited by its definition of effective boundary condition to apply to its *local problem lambda* and *local problem source*. Indeed, the space Λ_l is spanned by $\mathbb{P}_l(\sigma)$ on each coarse face $\sigma \in F_H$, independently from the fine scale information, hence, the introduction of weighting scheme for the space Λ_l. In order to better fit the heterogeneous media, we can modify the native version of each algorithm. MsFv can make the use of smoothing steps in order to converge to the desired fine scale solution. Based on the native MsFv, the neglected fluxes from the localization assumption can be estimated from the residual.
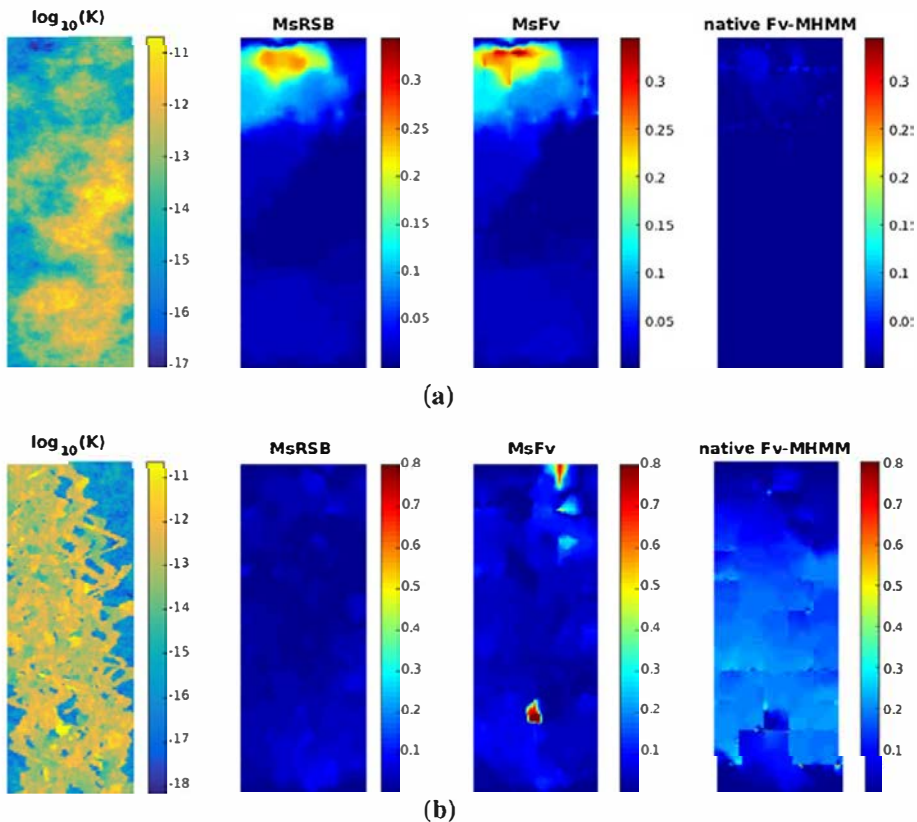
Fig. 6 Native methods: normalized error $\epsilon_1(x)$ for the 13th and 84th SPE layer

	MsFv	MsRSB	Native Fv-MHMM
(a) Native methods: ϵ_{L_2} error report for 13th layer			
Mesh 10×11	0.0216	0.0209	0.00249
Mesh 5×11	0.0236	0.0220	0.00226
(b) Native methods: ϵ_{L_2} error report for 84th layer			
Mesh 10×11	NC	0.0111	0.0322
Mesh 5×11	0.0390	0.0124	0.0585

Table 2 Native methods: L_2-norm error report for native methods (i.e., single stage MsFv or MsRSB and Fv-MHMM without weighing scheme). NC stands for non-converged solution

4.2 Improved Implementations Versions of the Multiscale Algorithms

In Fig. 8 is reported $\epsilon_1(x)$ for MsRSB and MsFv with 25 cycles and 100 cycles of smoother-multiscale solution. The $\epsilon_1(x)$ levels for transmissivity weighted (tw) and multiscale two point flux approximation (mstpfa) FV-MHMM are also reported.

On the 13th layer (Fig. 8a), the smoothing cycles significantly improved the accuracy of the solution. Similarly, noticing the scales, we can verify that tw and mstpfa weighting schemes have positive impact on the accuracy. This result is supported by the report on L_2-norm error synthesized in Table 4a. A hundred cycles drop the error levels by two orders of magnitude, while weighting scheme produces between one and half to two times less error.
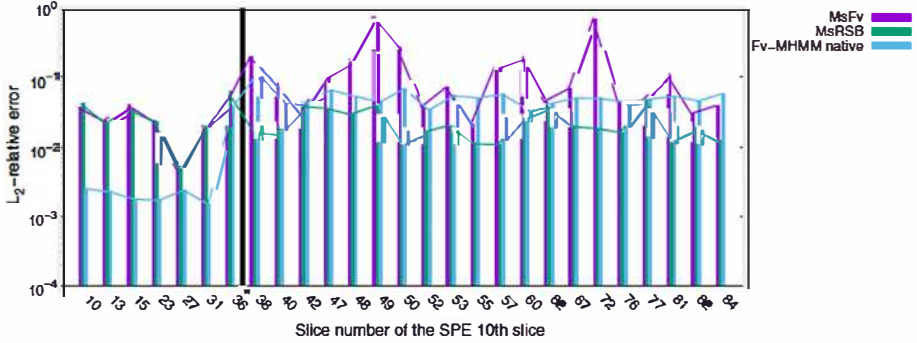
Fig. 7 Native methods: relative $norm - L_2$ errors for all the SPE layers

Table 3 Native methods: L_2-norm statistics per facies

	Top layers	Bottom layers
MsFv	0.0246 (0.0128)	0.150 (0.196)
MsRSB	0.0242 (0.0125)	0.0246 (0.0138)
Native FvMHMM	2.03 (0.41) $\times 10^{-3}$	0.0520 (0.0166)

Values are presented as mean (standard deviation)

On the 84th layer (Fig. 8b), MsFv and MsRSB efficiently smooth out their errors, while weighting schemes for FV-MHMM allow to reduce the error in better representing the flow at the boundaries when computing basis functions. Looking at the report on Table 4b, the cycles significantly improve the accuracy of the multiscale approximation, especially for MsFv. Regarding, the weighting schemes effects, it can be noticed that mstpfa scheme is more efficient on 5×11 coarse discretization than on 10×11 discretization. It can be explained by the fact that it includes more details of the flow by considering larger neighboring coarse cells in its computation.

From the summary plot Fig. 9 and statistical report Table 5, we can observe that on the top layers, the smoother-multiscale solution cycles for MsFv and MsRSB result in error levels one order of magnitude smaller than what can be achieved with tw and mstpfa FV-MHMM. On the channelized medium, MsRSB cycled and weighted formulations achieved to reach the same accuracy, when comparing their norm-L_2 error levels.

5 The Slanted Case Study

The second test case is a bottom to top cross-flow performed on a 75 by 5 ft slanted permeability field (see Table 6). The main feature of this case is the stripes of low and high permeable regions which are non aligned with the cartesian grids. Ten realizations have been drawn with the two non-dimensional correlation lengths $\lambda_1 = 0.5$ and $\lambda_2 = 0.02$. The variance of K is set such as $\sigma(\log(k)) = 3.0$. An example of such a realization is given on Fig. 10.

As before, error levels are reported in terms of mean and standard deviations in Table 7. From these data, the reader can observe that on *native* formulations, both MsFv and MsRSB have their error level reduce when considering a refined coarse discretization. Switching to the improved version of algorithm, it can be noticed that too fine coarse mesh for MsFv deteriorates the accuracy as it includes less details about the surrounding flows. Apart from
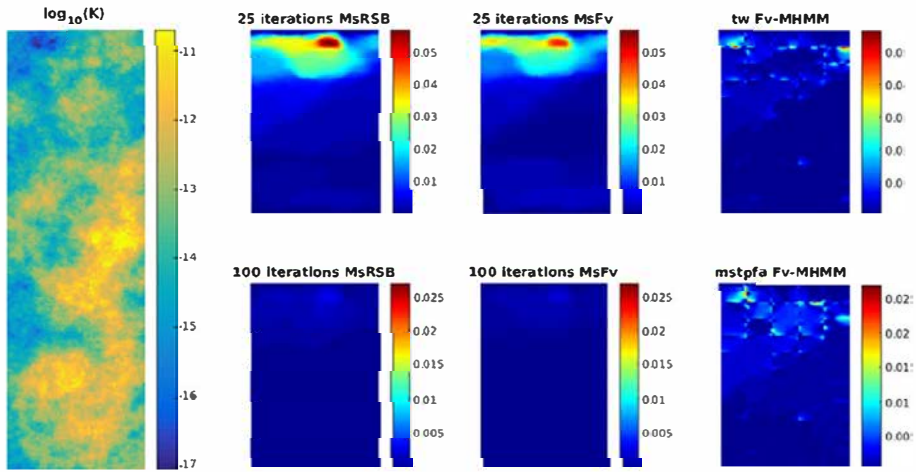
(a)
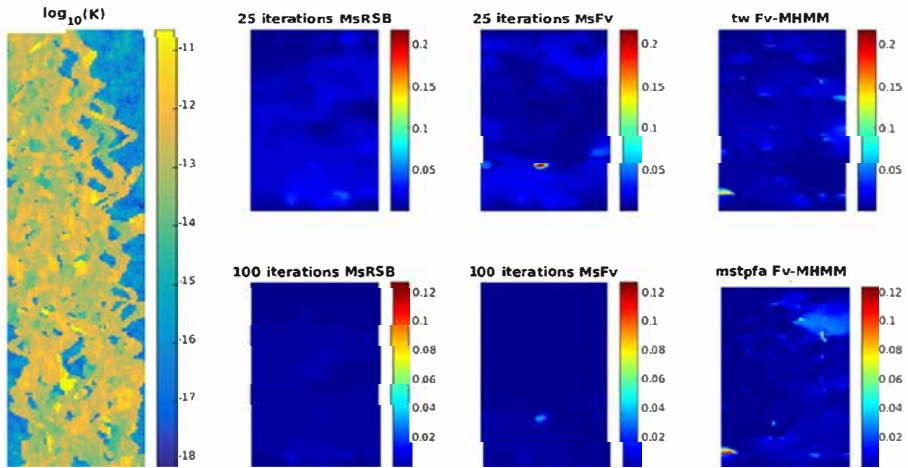
(b)

Fig. 8 Improved methods: normalized error $\epsilon_1(x)$ for the 13th and 84th SPE layer

Table 4 Improved methods: L_2-norm error report for improved methods (i.e., 100 smoother-multiscale solution cycles for MsFv or MsRSB and FV-MHMM with tw and mstpfa weighting schemes)

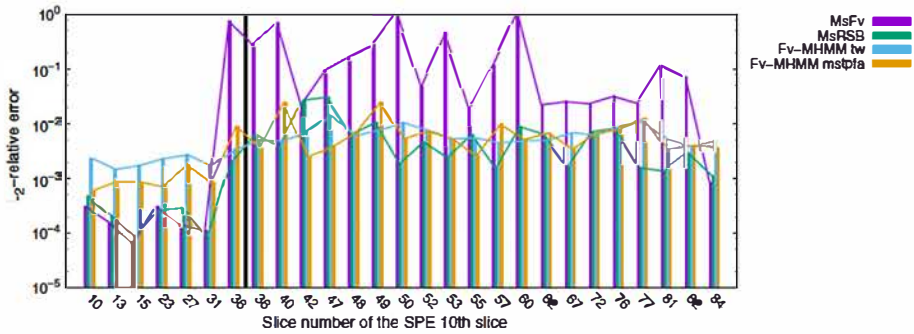|	MsFv	MsRSB	tw FV-MHMM	mstpfa FV-MHMM
(a) Improved methods: L_2-norm error report for 13th layer				
Mesh 10×11	3.21×10^{-5}	2.55×10^{-5}	1.14×10^{-3}	9.30×10^{-4}
Mesh 5×11	2.11×10^{-4}	1.58×10^{-4}	1.46×10^{-3}	8.53×10^{-4}
(b) Improved methods: L_2-norm error report for 84th layer				
Mesh 10×11	NC	4.72×10^{-4}	3.25×10^{-3}	3.24×10^{-3}
Mesh 5×11	8.55×10^{-4}	1.11×10^{-3}	4.73×10^{-3}	3.67×10^{-3}

NC stands for non-converged solution

Fig. 9 Improved methods: relative norm-L_2 errors for all the SPE layers

Table 5 Improved methods: L_2-norm statistics per facies

	Top layers	Bottom layers
MsFv	$1.82\,(1.02) \times 10^{-4}$	$0.255\,(0.347)$
MsRSB	$2.35\,(1.47) \times 10^{-4}$	$6.78\,(7.82) \times 10^{-3}$
tw Fv-MHMM	$2.03\,(0.47) \times 10^{-3}$	$6.56\,(2.68) \times 10^{-3}$
mstpfa Fv-MHMM	$9.30\,(4.17) \times 10^{-4}$	$7.56\,(6.28) \times 10^{-3}$

Values are presented as mean (standard deviation)

Table 6 Simulation conditions for the slanted test case

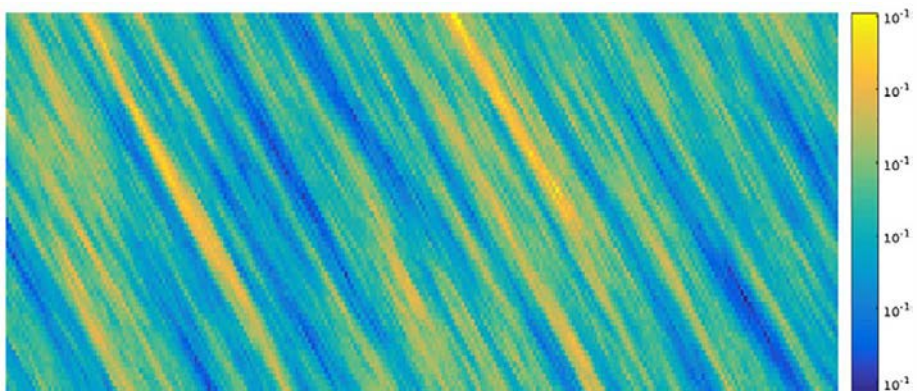|	
Physical dimensions of the slanted test case	$75\,\text{ft} \times 5\,\text{ft}$
Fine grid: number of cells (x, y)	$256 \times 64\,\text{cells}$
Coarse grid: number of cells (x, y)	$32 \times 16\,\text{cells}/8 \times 4\,\text{cells}$
Pressure drop imposed in y-direction	$\Delta p = 1\,\text{Pa}$

Fig. 10 Example of a log-permeability field map in the slanted case

that, the cycles are once again efficient in dropping the error level up to two orders of magnitude. On the FV-MHMM side, weighting schemes are counterproductive. The slanted heterogeneous features induce a corner flow which is badly estimates by both schemes. It

Table 7 L_2-norm statistics on slanted realizations

	8×4	32×16
(a) Native methods		
MsFv	0.0576 (0.0224)	0.0526 (0.0202)
MsRSB	0.0365 (0.00457)	0.0180 (0.00257)
Native FV-MHMM	0.0164 (0.00325)	$5.73 (1.51) \times 10^{-3}$
(b) Improved methods		
MsFv	$3.62 (1.31) \times 10^{-3}$	$4.42 (1.12) \times 10^{-2}$
MsRSB	$4.10 (1.37) \times 10^{-3}$	$9.24 (3.97) \times 10^{-5}$
tw FV-MHMM	$2.15 (0.167) \times 10^{-2}$	$1.79 (0.156) \times 10^{-2}$
mstpfa FV-MHMM	$8.39 (2.09) \times 10^{-3}$	$8.75 (0.625) \times 10^{-3}$

Values are presented as mean (standard deviation)

results in less accurate solution. Considering this analysis of the results on the slanted case, an alternative approach for the FV-MHMM method (different of tw or mstpfa approaches) will be needed to obtain results comparable to other methods. For example, a possibility we are exploring is to build an adaptive formulation of the FV-MHMM formulation, in the same vein as adaptive finite elements, which could be combined with tw or mstpfa weighting schemes approaches.

6 Conclusion

In this paper, three different multiscale methods FV-MHMM, MsFv and MsRSB have been tested using several different configurations. The MsFv and MsRSB methods are currently the most widely used in the reservoir simulation community (Moyner et al. 2015; Lunati et al. 2009). Their performances have been cross-compared on 2D cases considering the number of iterations they use solving the system, as a raw indicator of their numerical efficiency. On log-normally distributed facies of the 10th SPE test case, MsFv and MsRSB share the same accuracy which is improved by two order of magnitude after few smoother-multiscale solution cycles. FV-MHMM has in-between performance in terms of accuracy and can improve slightly its results by the use of weighting schemes (tw or mstpfa). The channelized type of medium challenges more the multiscale methods tested. MsFv has to work with a coarse enough mesh to be sure to find a solution on all layers as already mentioned in Wang et al. (2014), Møyner and Lie (2016). Considered as a single stage multiscale solver, MsRSB finds solution with one order of magnitude lower error than the native form of FV-MHMM. If fewer cycles for MsRSB and weighting scheme for FV-MHMM are used, the error levels are lowered by one order of magnitude.

In a last part, a slanted permeability case was studied: with this type of heterogeneity, the FV-MHMM struggles to correctly reproduce fine scale fluxes. On the other hand, MsRSB and MsFv, respectively, in their cycled version, correctly reproduce the fine scale details, as their solutions converge to the fine scale solution. This slanted permeability test highlights a limitation of FV-MHMM, which has to do with the proper definition of effective boundary conditions for its basis functions. Indeed, either MsFv by its dual-primal mesh definition which leads to a multiple point coarse stencil, or MsRSB by its definition of overlapping areas, include more details of the surrounding flow when computing their basis functions. The construction of the weighting schemes for the FV-MHMM aims at enhancing this bound-

ary condition to better fit the surrounding flow. In the slanted test case, since the weighting schemes do not improve the solution accuracy, another idea would be to develop an adaptive formulation of the FV-MHMM by analogy with adaptive finite elements. This work is ongoing.

On the other hand, MsRSB and MsFv methods have been enriched by many improvements. They have already been used to treat 3D cases with more elaborate fluid models (Møyner et al. 2017; Hilden et al. 2016). For instance, capillary and gravity effects, black oil model and fractured medium, have all been implemented (Møyner et al. 2016; Bosma et al. 2017; Shah et al. 2016; Lunati and Jenny 2008). MsRSB is also adapted to unstructured meshes (Møyner 2014). Furthermore, after having been reformulated as algebraic solvers, MsRSB and MsFv are now considered in the most recent works as a non-symmetric preconditioner for the fine scale problem using GMRES solvers (Møyner 2014; Manea et al. 2016). Once formulated in its algebraic form, FV-MHMM could be used as a preconditioning technique, in the same fashion as in the work of (Lunati and Lee 2009). This will be a forthcoming line of research.

A Complexity Comparison

Following the steps which are written in Jenny et al. (2003) for complexity analysis of MsFv multiscale algorithm, we remind here the results for FV-MHMM (Franc et al. 2017) and proposed the same kind of analysis for MsRSB. The notations introduced are presented in Table 8.

Assuming that $t_1(n) \sim ct_{m}n^{\alpha}$ where t_{m} is the time spent for one multiplication, c and α are constants depending on the solvers. This complexity analysis neglects time spent in the reconstruction of the pressure and the fluxes. For MsFv, reproducing the analysis of Jenny et al. (2003), it leads to:

Table 8 Parameters

n_{v}	Number of volumes in the fine grid
N_{v}	Number of volumes in the coarse grid
N_{n}	Number of nodes in the coarse grid
N_{f}	Number of faces in the coarse grid
γ	Coarsening ratio $\sim n_{v}/N_{v}$
a_{n}	Number of coarse volumes adjacent to a coarse node
a_{v}	Number of coarse volumes adjacent to a coarse volume
n_{it}	Number of iterations spent in smoothing basis function for MsRSB
$t_1(n)$	Time to invert a linear system with n unknowns

N_{v}	n_{v}	γ	d	a_{v}	a_{v}	N_{n}	n_{it}
9	3600	400	2	8	4	12	100

$$t_{\text{MsFv1}} \approx N_n a_n c t_m \gamma^\alpha,$$
$$t_{\text{MsFv2}} \approx N_v (a_v + 1) c t_m \gamma^\alpha,$$
$$t_{\text{MsFv3}} \approx c t_m N_v^\alpha$$

with the step MsFv1, the time spent in constructing the basis function on the dual grid; MsFv2, the time spent building coarse scale equivalent transmissivities on the coarse grid and MsFv3, the time needed to invert the coarse system.

In the same manner, FV-MHMM can be cast into three main steps:

$$t_{\text{LLP}} \approx 2d(l+1)N_v c t_m \gamma^\alpha,$$
$$t_{\text{LSP}} \approx N_v c t_m \gamma^\alpha,$$
$$t_{\text{GP}} \approx c t_m [N_v + (l+1)N_f]^\alpha$$

where d is the dimension number, l the order of the polynomial space used to approximate Λ_H and considering an average number of faces as $N_f \approx d(N_v^{1/d}+1)\prod_{i=1}^{d-1} N_v^{1/d}$. The LLP step denotes the time spent in the construction of Lagrange multipliers-related basis functions; LSP, the time spent in the construction of source term-related basis functions and GP the time spent inverting the global problem.

For the MsRSB, it has to be noted that its basis functions computations do not require inverting any operator. Indeed, in the Jacobi smoother formulation, only diagonal preconditioner D^{-1} is required, which is trivially inverted. It left us with:

$$t_{\text{MsRSB1}} \approx n_{it}(\gamma_{\text{overlap}} + \gamma)N_v t_m$$
$$t_{\text{MsRSB2}} \approx n_{it}\gamma_{\text{overlap}}N_v t_m$$
$$t_{\text{MsRSB3}} \approx c t_m N_v^\alpha$$

with the step MsRSB1 stands for the time spent in smoothing the basis functions on the overlapping supports; MsRSB2 represents the time spent restricting the spreading of the basis functions to ensure mass conservation and, as in MsFv, MsRSB3, the time needed to invert the coarse system. Estimating the overlap size is done counting nodes nu_n, edges nu_e and faces nu_f of a coarse cell depending on d (see Table 9). To define γ_{overlap}, let us introduce $\overline{nc}$ the mean number of fine cells per dimension embedded in a coarse cell, that is do say $\overline{nc} \approx \gamma^{1/d}$. Then, the overlapping area is counted as:

$$\gamma_{\text{overlap}} = nu_f \overline{nc}^{(d-1)}\left(\frac{\overline{nc}}{2}\right)$$
$$+ nu_e \overline{nc}^{(d-2)}\left(\frac{\overline{nc}}{2}\right)^2$$
$$+ nu_n \left(\frac{\overline{nc}}{2}\right)^d$$

Table 9 Counting for MsRSB overlap

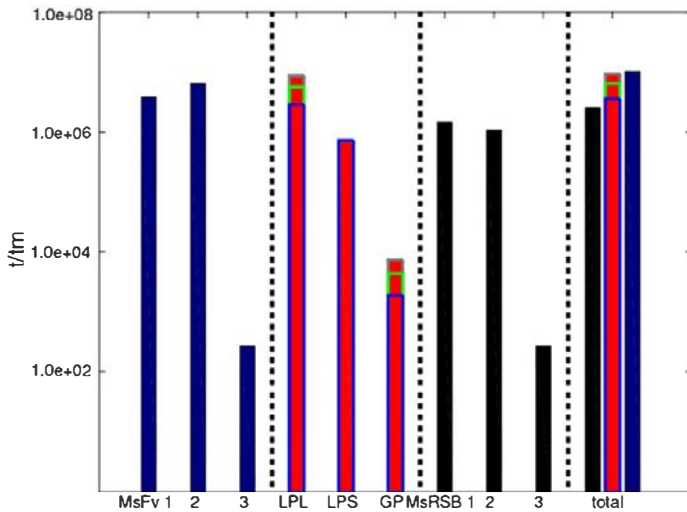|	$d = 1$	$d = 2$	$d = 3$
nu_f	2	4	6
nu_e	0	0	12
nu_n	0	4	8

Fig. 11 Complexity plot for Table 8 parameters. From left to right, the first region stands for MsFv, the second for FV-MHMM, the third for MsRSB. The right most region represents the total amount of computational time spent for each method

Moreover, the step MsFv1 and step MsFv2 are reported to be parallelizable for the MsFv method (Jenny et al. 2003). As for the FV MHMM, all the local problems lambda (LLP) and local problems source (LSP) are independent from each others and therefore can be treated in parallel. Moreover, the TPFA matrix for a selected coarse cell has to be generated only one time and can be used for solving both LLP and LSP associated with this coarse cell (see Fig. 11).

References

Aarnes, J.E.: On the use of a mixed multiscale finite element method for greaterflexibility and increased speed or improved accuracy in reservoir simulation. Multiscale Model. Simul. 2(3), 421–439 (2004)

Arbogast, T.: Implementation of a locally conservative numerical subgrid upscaling scheme for two-phase Darcy flow. Comput. Geosci. 6(3–4), 453–481 (2002)

Arbogast, T., Cowsar, L.C., Wheeler, M.F., Yotov, I.: Mixed finite element methods on nonmatching multiblock grids. SIAM J. Numer. Anal. 37(4), 1295–1315 (2000)

Arbogast, T., Pencheva, G., Wheeler, M.F., Yotov, I.: A multiscale mortar mixed finite element method. Multiscale Model. Simul. 6(1), 319–346 (2007)

Bosma, S., Hajibeygi, H., Tene, M., Tchelepi, H.A.: Multiscale finite volume method for discrete fracture modeling on unstructured grids (ms-dfm). J. Comput. Phys. 351, 145–164 (2017)

Castelletto, N., Hajibeygi, H., Tchelepi, H.A.: Multiscale finite-element method for linear elastic geomechanics. J. Comput. Phys. 331, 337–356 (2017)

Christie, M., Blunt, M., et al.: Tenth spe comparative solution project: a comparison of upscaling techniques. In: SPE Reservoir Simulation Symposium, Society of Petroleum Engineers (2001)

Efendiev, Y., Galvis, J., Hou, T.Y.: Generalized multiscale finite element methods (gmsfem). J. Comput. Phys. 251, 116–135 (2013)

Franc, J., Jeannin, L., Debenest, G., Masson, R.: Fv-mhmm method for reservoir modeling. Comput. Geosci. 21(5–6), 895–908 (2017)

Hajibeygi, H., Jenny, P.: A general multiscale finite-volume method for compressible multiphase flow in porous media. In: ECMOR XI-11th European Conference on the Mathematics of Oil Recovery (2008)

Hajibeygi, H., Jenny, P.: Adaptive iterative multiscale finite volume method. J. Comput. Phys. 230(3), 628–643 (2011)

Hajibeygi, H., Bonfigli, G., Hesse, M.A., Jenny, P.: Iterative multiscale finite-volume method. J. Comput. Phys. 227(19), 8604–8621 (2008)

Hajibeygi, H., Lunati, I., Lee, S.H.: Error estimate and control in the msfv method for multiphase flow in porous media. In: Proceedings of XVIII International Conference on Computational Methods in Water Resources (CMWR XVIII), Barcelona, Spain (2010)

Harder, C., Paredes, D., Valentin, F.: A family of multiscale hybrid-mixed finite element methods for the Darcy equation with rough coefficients. J. Comput. Phys. **245**, 107–130 (2013)

Harder, C., Paredes, D., Valentin, F.: On a multiscale hybrid-mixed method for advective-reactive dominated problems with heterogeneous coefficients. Multiscale Model. Simul. **13**(2), 491–518 (2015)

Hilden, S.T., Møyner, O., Lie, K.A., Bao, K.: Multiscale simulation of polymer flooding with shear effects. Transp. Porous Media **113**(1), 111–135 (2016)

Hou, T.Y., Wu, X.H.: A multiscale finite element method for elliptic problems in composite materials and porous media. J. Comput. Phys. **134**(1), 169–189 (1997)

Jenny, P., Lunati, I.: Modeling complex wells with the multi-scale finite-volume method. J. Comput. Phys. **228**(3), 687–702 (2009)

Jenny, P., Lee, S., Tchelepi, H.A.: Multi-scale finite-volume method for elliptic problems in subsurface flow simulation. J. Comput. Phys. **187**(1), 47–67 (2003)

Lee, S.H., Zhou, H., Tchelepi, H.A.: Adaptive multiscale finite-volume method for nonlinear multiphase transport in heterogeneous formations. J. Comput. Phys. **228**(24), 9036–9058 (2009)

Lie, K.A.: An introduction to reservoir simulation using matlab: user guide for the matlab reservoir simulation toolbox (mrst). sintef ict (2014)

Lunati, I., Jenny, P.: The multiscale finite volume method. In: 10th European Conference on the Mathematics of Oil Recovery (ECMOR X) (2006a)

Lunati, I., Jenny, P.: Multiscale finite-volume method for compressible multiphase flow in porous media. J. Comput. Phys. **216**(2), 616–636 (2006b)

Lunati, I., Jenny, P.: Multiscale finite-volume method for density-driven flow in porous media. Comput. Geosci. **12**(3), 337–350 (2008)

Lunati, I., Lee, S.H.: An operator formulation of the multiscale finite-volume method with correction function. Multiscale Model. Simul. **8**(1), 96–109 (2009)

Lunati, I., Tyagi, M., Lee, S.: Multiscale finite volume method for reservoir simulation, Patent (2009)

Lunati, I., Tyagi, M., Lee, S.H.: An iterative multiscale finite volume algorithm converging to the exact solution. J. Comput. Phys. **230**(5), 1849–1864 (2011)

Manea, A.M., Sewall, J., Tchelepi, H.A., et al.: Parallel multiscale linear solver for highly detailed reservoir models. SPE J. **21**(06), 2–62 (2016)

Møyner, O.: Construction of multiscale preconditioners on stratigraphic grids. In: ECMOR XIV-14th European Conference on the Mathematics of Oil Recovery (2014)

Møyner, O., Lie, K.A.: A multiscale two-point flux-approximation method. J. Comput. Phys. **275**, 273–293 (2014)

Møyner, O., Lie, K.A.: A multiscale restriction-smoothed basis method for high contrast porous media represented on unstructured grids. J. Comput. Phys. **304**, 46–71 (2016)

Moyner, O., Lie, K., Natvig, J.: Adaptive multiscale multi-fidelity reservoir simulation, Patent (2015)

Møyner, O., Lie, K.A., et al.: A multiscale restriction-smoothed basis method for compressible black-oil models. SPE J. **21**(06), 2–079 (2016)

Moyner, O., Tchelepi, H., et al: A multiscale restriction-smoothed basis method for compositional models. In: SPE Reservoir Simulation Conference, Society of Petroleum Engineers (2017)

Raviart, P.-A., Thomas, J.M.: Primal hybrid finite element methods for 2nd order elliptic equations. Math. Comput. **31**(138), 391–413 (1977a). http://www.ams.org/publications/journals/journalsframework/mcom

Raviart, P.-A., Thomas, J.-M.: A mixed finite element method for 2-nd order elliptic problems. In: Mathematical Aspects of Finite Element Methods, pp. 292–315. Springer (1977b)

Shah, S., Møyner, O., Tene, M., Lie, K.A., Hajibeygi, H.: The multiscale restriction smoothed basis method for fractured porous media (f-msrsb). J. Comput. Phys. **318**, 36–57 (2016)

Ţene, M., Wang, Y., Hajibeygi, H.: Adaptive algebraic multiscale solver for compressible flow in heterogeneous porous media. J. Comput. Phys. **300**, 679–694 (2015)

Ţene, M., Al Kobaisi, M.S., Hajibeygi, H.: Algebraic multiscale method for flow in heterogeneous porous media with embedded discrete fractures (f-ams). J. Comput. Phys. **321**, 819–845 (2016)

Vaněk, P., Mandel, J., Brezina, M.: Algebraic multigrid by smoothed aggregation for second and fourth order elliptic problems. Computing **56**(3), 179–196 (1996)

Wang, Y., Hajibeygi, H., Tchelepi, H.A.: Algebraic multiscale solver for flow in heterogeneous porous media. J. Comput. Phys. **259**, 284–303 (2014)

Zhou, H., Tchelepi, H.A., et al.: Two-stage algebraic multiscale linear solver for highly heterogeneous reservoir models. SPE J. **17**(02), 523–539 (2012)